

4. VNSの長期効果と有効性の判定

Q. VNSの長期発作抑制効果は期待できるか？ また無効と判断するまでにどの程度の期間、治療を継続するべきか？

1. VNSの発作抑制率は治療継続によりおよそ2年間増大し、その後安定して継続すると期待できる。【推奨度C】
2. VNSが無効と判断するまでに2年間は治療を継続する。【推奨度C】

解説

前項で取り上げた二つの無作為対照試験の治療期間は3ヶ月と短かったが、その後のオープンラベル追跡調査により、発作が50%以上減少する患者の率は、治療期間1年で37%、2年43%、3年43%と、年単位での治療継続で徐々に発作抑制効果が徐々に高まり、発作減少率はおよそ50%で安定する³¹⁰⁾。なお、年齢や発作型あるいはてんかん分類によって長期成績に大きな差はみられていない³¹⁰⁾。

VNSが無効と判断する基準に関する研究報告はないが、上記の長期治療効果の報告から、2年間は治療の継続が必要と考えられる。

5. VNSの術前検査

Q. VNS施行前にはどのような検査が必要か？

根治的な開頭手術の適否を精査した上で、VNSの適応を判断する。【推奨度C】

解説

VNSの適応判断には、開頭手術の術前精査に準じた検査を行う。VNSのてんかん発作に対する効果は緩和的であり、開頭による焦点切除術に根治的效果が期待できる場合は、原則的に開頭手術の施行を検討すべきである。ビデオ脳波などの基本的な術前検査を省略したため、適応外の患者にVNSが行われたという報告もある¹¹⁾。

6. VNS刺激装置の植込手術

Q. VNSに用いる刺激装置の植込手術はどのように行うか。

VNSには専用の植込型刺激装置システムを用いる。装置の植込手術は、原則的に全身麻酔下で行い、パルスジェネレータを左前胸部皮下脂肪層に、らせん電極を左迷走神経に留置する。【推奨度C】

解説

装置の植込手術は、製造元が作成した専用の埋込型刺激装置システムのマニュアルに従って行う。試験刺激中の一過性徐脈・心停止(0.2%)や術後一過性の反回神経麻痺(1%)など手術合併症を避けるため、適切な部位での迷走神経確保や愛護的な電極留置操作を行う¹²⁾。

パルスジェネレータの電源寿命は現在のところ約6年で、治療継続のためにはパルスジェネレータの交換手術が必要である。電源寿命による装置停止による発作の再発や悪化があり得るので、製造元マニュアルに従った定期的なデバイス診断により予想残存寿命を確認し、装置停止前に警告に従ってパルスジェネレータを交換する¹³⁾¹⁰⁾。

7. VNS治療の方法

Q. VNSの刺激治療はどのように行うか。

VNSは、原則として植込手術の2週間後から開始する。弱い刺激強度から開始し、副作用の発現に注意しながら徐々に刺激強度を上げる。【推奨度C】

解説

刺激治療は装置植込の約2週間後から開始する。標準的には、0.25 mA、500 usec、30 Hz、30秒ON、5分

OFF、で開始し、副作用の出現しない範囲で、発作に対する効果をみながら最大 3.50 mA まで上げてゆく¹⁵⁾。効果がなければ、duty cycle (1 サイクルのうち ON 時間の占める割合) も上げてゆく。至適条件は患者によって異なり、試行錯誤が必要である^{15,16)}。

8. VNS の副作用

Q. 刺激開始時の副作用はどのようなものがあり、どう対応するか。

VNS 刺激開始時の副作用は、咳、嘔声、咽頭部不快感、嚥下障害などである。忍容できない副作用には刺激強度を下げることで対応する。【推奨度 C】

解説

刺激治療に伴う副作用は、咳、嘔声、咽頭部不快感、嚥下障害などだが、これらは可逆的で、忍容できない副作用には刺激強度を下げて対応する。副作用の発現率は治療継続とともに減少する²⁹⁾。突然の動作不良など緊急時には、製造元マニュアルに従って装置を緊急停止させ、直ちに条件設定の可能な医療施設を受診させる。

9. VNS と医療機器・電気電子機器との相互作用

Q. VNS と医療機器・電気電子機器との相互作用は問題にならないか？ 特に MRI についてはどうか？

1. VNS 治療中の患者における頭部 MRI 検査は、頭部撮像に限り製造元マニュアルに従って施行可能である。【推奨度 C】
2. 日常生活における電気電子機器からの影響は最小限のものだが、強い磁場からは 15 cm 以上離れる。【推奨度 C】

解説

VNS 治療中の患者に対する MRI 検査は、3 テスラ以下 (3 テスラを含む) の頭部コイルを用いた頭部撮像に限り、刺激を中断し製造元マニュアルの推奨条件下に施行可能である¹⁷⁾。

脳磁図は安全に施行できるが、ノイズ対策が必要である^{18,19)}。

家電製品、携帯電話、空港の金属探知機や商店の盗難防止センサーなどからは VNS 装置は影響を受けない。ただし、非常に強い磁石は刺激開始や中止の誤指令を出す可能性があり、製造元のマニュアルでは、大きなスピーカーやバイブレーターなど強い磁石を内蔵する機器からは 15 cm 以上離れるよう推奨している。

10. 効果がないと判断する場合

Q. VNS が無効と判断した場合の対処方法は？

1. 忍容範囲で刺激条件を最大まで上げ、または 2 年以上の継続治療を行った上で無効と判断された場合、刺激を停止し、てんかん発作の経過を観察する。【推奨度 C】
2. 患者または家族の希望により装置の抜去を検討する。【推奨度 C】

解説

発作と他の症状への効果より総合的に VNS が無効と判断した場合の対処方法に関する研究報告はないが、刺激を停止することを考慮する。一方、パルスジェネレータの電源寿命が尽きた患者では、てんかん発作の悪化があり得る^{13,14)}。したがって、刺激条件を下げた場合、停止した場合には、てんかん発作の悪化がないか経過観察を行う。

患者・家族が希望すれば装置の抜去を検討する。VNS 装置抜去手術のリスクに関する研究報告はないが、パルスジェネレータ抜去手術の合併症発生率はきわめて低いと予想される。一方、迷走神経に留置した電極の抜去手術は、電極と神経の癒着から、神経損傷の相応なリスクを有するが²⁰⁾、安全な抜去が可能との報告もある²¹⁾。

11. その他

Q. VNS 施行についてその他の留意事項は何か？

本治療の施行に際しては、てんかん診療に関する十分な知識と経験を有するてんかん専門医が、技術講習会を受講し、迷走神経刺激療法資格認定委員会による認定を受けた後に施行する（日本てんかん学会、日本てんかん外科学会、日本脳神経外科学会合同の迷走刺激療法認定委員会によるガイドラインを参照のこと）

解説

承認にあたり、3学会ガイドラインが策定された。日本でVNSを施行する場合にはこれに準拠することが望ましい。ただし、これは3年間で見直すことになっており、変更される可能性がある。

参考 平成22年1月8日薬事承認時に認定委員会によって策定されたガイドライン

1. 本療法の適応判断と刺激装置植込術は、日本てんかん学会専門医ならびに日本脳神経外科学会専門医の両資格を有するてんかん外科治療を専門に行っている医師によって、またはその指導の下に行われるべきものとする。
2. 本療法の開始後の刺激条件の調整や、治療効果および有害事象の追跡調査は、日本てんかん学会専門医（すべての診療科を含む）またはその指導の下に行われるべきものとする。
3. 本療法を行う医師（1項、2項に該当する医師）は、初回施行前に、日本てんかん学会、日本てんかん外科学会、日本脳神経外科学会の共催による講習会を受講しなければならない。
4. 刺激装置植込術を行う医師は、受講資格として前年1年間のてんかん外科手術症例リストの申告を必要とする。
5. 受講修了者は、3学会合同の認定委員会によって認定証が授与され、本療法の実施資格が認められる。なお、認定は認定委員会によって見直される場合がある。

参考 平成22年1月8日薬事法承認における目的・効果・承認条件

使用目的、効能又は効果

迷走神経刺激装置 VNS システムは、薬剤抵抗性の難治性てんかん発作を有するてんかん患者（開頭手術が奏功する症例を除く）の発作頻度を軽減する補助療法として、迷走神経を刺激する電気刺激装置である。

承認条件

1. てんかん治療に対する十分な知識・経験を有する医師が、難治性てんかん発作に対する本品を用いた迷走神経刺激治療に関する講習の受講等により、本品の有効性及び安全性を十分に理解し、手技及び当該治療に伴う合併症等に関する十分な知識・経験を得た上で、適応を遵守して用いるように必要な措置を講じること。
2. 使用成績調査により、登録症例（国内治験症例を含む。）及び全ての小児症例の長期予後について、経年解析結果を報告するとともに、必要により適切な措置を講じること。

文 献

- 1) The Vagus Nerve Stimulation Study Group. A randomized controlled trial of chronic vagus nerve stimulation for treatment of medically intractable seizures. The Vagus Nerve Stimulation Study Group. *Neurology* 1995; 45: 224-30. [I]
- 2) Handforth A, DeGiorgio CM, Schachter SC, Uthman BM, Naritoku DK, Tecoma ES, Henry TR, Collins SD, Vaughn BV, Gilmartin RC, Labar DR, Morris GL, 3rd, Salinsky MC, Osorio I, Ristanovic RK, Labiner DM, Jones JC, Murphy JV, Ney GC, Wheless JW. Vagus nerve stimulation therapy for partial-onset seizures: a randomized active-control trial. *Neurology* 1998; 51: 48-55. [I]
- 3) Clark KB, Naritoku DK, Smith DC, Browning RA, Jensen RA. Enhanced recognition memory following vagus nerve stimulation in human subjects. *Nat Neurosci* 1999; 2: 94-8. [I]
- 4) Elger G, Hoppe C, Falkai P, Rush AJ, Elger CE. Vagus nerve stimulation is associated with mood improvements in epilepsy patients. *Epilepsy Res* 2000; 42: 203-10. [II]
- 5) Harden CL, Pulver MC, Ravdin LD, Nikolov B, Halper JP, Labar DR. A Pilot Study of Mood in Epilepsy Patients

- Treated with Vagus Nerve Stimulation. *Epilepsy Behav* 2000; 1: 93-99. [II]
- 6) Murphy JV. Left vagal nerve stimulation in children with medically refractory epilepsy. The Pediatric VNS Study Group. *J Pediatr* 1999; 134: 563-6. [III]
 - 7) Blount JP, Tubbs RS, Kankirawatana P, Kiel S, Knowlton R, Grabb PA, Bebin M. Vagus nerve stimulation in children less than 5 years old. *Childs Nerv Syst* 2006; 22: 1167-9. [III]
 - 8) Elliott RE, Rodgers SD, Bassani L, Morsi A, Geller EB, Carlson C, Devinsky O, Doyle WK. Vagus nerve stimulation for children with treatment-resistant epilepsy: a consecutive series of 141 cases. *J Neurosurg Pediatr* 2011; 7: 491-500. [III]
 - 9) Morris GL, 3rd, Mueller WM. Long-term treatment with vagus nerve stimulation in patients with refractory epilepsy. The Vagus Nerve Stimulation Study Group E01-E05. *Neurology* 1999; 53: 1731-5. [III]
 - 10) Elliott RE, Morsi A, Tanweer O, Grobelny B, Geller E, Carlson C, Devinsky O, Doyle WK. Efficacy of vagus nerve stimulation over time: review of 65 consecutive patients with treatment-resistant epilepsy treated with VNS > 10 years. *Epilepsy Behav* 2011; 20: 478-83. [III]
 - 11) Attarian H, Dowling J, Carter J, Gilliam F. Video EEG monitoring prior to vagal nerve stimulator implantation. *Neurology* 2003; 61: 402-3. [IV]
 - 12) DeGiorgio CM, Amar A, Apuzzo MLJ. Surgical anatomy, implantation technique, and operative complications. In: *Vagus Nerve Stimulation*. Vol. S.C. Schachter, D. Schmidt, ed. Martin Dunitz Ltd, London; 2001: pp. 31-50. [IV]
 - 13) Tatum WOT, Ferreira JA, Benbadis SR, Heriaud LS, Gieron M, Rodgers-Neame NT, Vale FL. Vagus nerve stimulation for pharmacoresistant epilepsy: clinical symptoms with end of service. *Epilepsy Behav* 2004; 5: 128-32. [III]
 - 14) Vonck K, Dedeurwaerdere S, De Groote L, Thadani V, Claeys P, Gossiaux F, Van Roost D, Boon P. Generator replacement in epilepsy patients treated with vagus nerve stimulation. *Seizure* 2005; 14: 89-99. [III]
 - 15) DeGiorgio C, Heck C, Bunch S, Britton J, Green P, Lancman M, Murphy J, Olejniczak P, Shih J, Arrambide S, Soss J. Vagus nerve stimulation for epilepsy: randomized comparison of three stimulation paradigms. *Neurology* 2005; 65: 317-9. [II]
 - 16) Bunch S, DeGiorgio CM, Krahl S, Britton J, Green P, Lancman M, Murphy J, Olejniczak P, Shih J, Heck CN. Vagus nerve stimulation for epilepsy: is output current correlated with acute response? *Acta Neurol Scand* 2007; 116: 217-20. [III]
 - 17) Benbadis SR, Nyhenhuis J, Tatum WOT, Murtagh FR, Gieron M, Vale FL. MRI of the brain is safe in patients implanted with the vagus nerve stimulator. *Seizure* 2001; 10: 512-5. [III]
 - 18) De Tiege X, Legros B, de Beeck MO, Goldman S, Van Bogaert P. Vagus nerve stimulation. *J Neurosurg Pediatr* 2008; 2: 375-7; author reply 377.
 - 19) Ross IB, Maleeva T, Sutherland WW. Vagus nerve stimulation. *J Neurosurg Pediatr* 2008; 2: 375; author reply 375.
 - 20) Vassilyadi M, Strawsburg RH. Delayed onset of vocal cord paralysis after explantation of a vagus nerve stimulator in a child. *Childs Nerv Syst* 2003; 19: 261-3. [IV]
 - 21) Espinosa J, Aiello MT, Naritoku DK. Revision and removal of stimulating electrodes following long-term therapy with the vagus nerve stimulator. *Surg Neurol* 1999; 51: 659-64. [IV]

Voxel-based comparison of preoperative FDG-PET between mesial temporal lobe epilepsy patients with and without postoperative seizure-free outcomes

Miwako Takahashi · Tsutomu Soma ·
Kensuke Kawai · Keitraro Koyama ·
Kuni Ohtomo · Toshimitsu Momose

Received: 21 May 2012 / Accepted: 24 June 2012 / Published online: 19 July 2012
© The Japanese Society of Nuclear Medicine 2012

Abstract

Objective This study aims to elucidate differences in preoperative cerebral glucose metabolism between patients who did and did not become seizure free after unilateral mesial temporal lobe epilepsy (mTLE) surgery. We hypothesized that regional glucose metabolism on preoperative fluorodeoxyglucose positron emission tomography (FDG-PET) in patients with seizure-free outcomes differed from that in patients who were not seizure free after appropriate epilepsy surgery for unilateral mTLE. In this study, we compared preoperative FDG-PET findings between these two patient groups by applying a statistical analysis approach, with a voxel-based Asymmetry index (AI), to improve sensitivity for the detection of hypometabolism.

Methods FDG-PET scans of 28 patients with medically refractory mTLE, of whom 17 achieved a seizure-free outcome (Engel class 1 a–b) during a postoperative follow-up period of at least 2 years, were analyzed retrospectively. Voxel values were adjusted by the AI method as well as the global normalization (GN) method. Two types of statistical

analysis were performed. One was a voxel severity analysis with comparison of voxel values at the same coordinate, and the other was extent analysis with comparison of the number of significant voxels in the anatomical areas pre-defined with Talairach's atlas.

Results In the voxel severity analysis, significant hypometabolism restricted to the ipsilateral temporal tip and hippocampal area was detected in the postoperative seizure-free outcome group as compared to controls. No significant area was detected in the non-seizure-free group as compared to controls (family-wise error corrected, $p < 0.05$). With extent analysis using a low threshold, the extents of hypometabolism in the ipsilateral hippocampal, frontal and thalamic areas were larger in the seizure-free than in the non-seizure-free group ($p = 0.01, 0.03$ and 0.01 , respectively.) On the other hand, in the contralateral frontal and thalamic areas, extents of hypometabolism were smaller in the seizure-free than in the non-seizure-free group ($p = 0.01$ and 0.01).

Conclusions We found the preoperative distribution of hypometabolism to differ between the two patient groups. Severe hypometabolism restricted to the unilateral temporal lobe, with ipsilateral dominant hypometabolism including mild decreases, may support the existence of an epileptogenic focus in the unilateral temporal lobe and a favorable seizure outcome after mTLE surgery.

Keywords Asymmetry index · FDG-PET · Mesial temporal lobe epilepsy · Postoperative outcome

Introduction

Epilepsy surgery is an important treatment for patients with medically refractory epilepsy. Surgery for temporal lobe

M. Takahashi · T. Soma · K. Koyama · K. Ohtomo ·
T. Momose (✉)
Department of Radiology, Graduate School of Medicine,
University of Tokyo, 3-1, Hongo 7-Chome, Bunkyo-ku,
Tokyo 113-8655, Japan
e-mail: tmomo-ty@umin.ac.jp

T. Soma
Software Development Group, Product Management and
Marketing Department, FUJIFILM RI Pharma Co., Ltd,
Tokyo, Japan

K. Kawai
Department of Neurosurgery, Graduate School of Medicine,
University of Tokyo, Tokyo, Japan

epilepsy (TLE) has become an established treatment [1]. While most patients benefit from this surgery, some suffer persistent seizures or recurrence [2].

Fluorodeoxyglucose positron emission tomography (FDG-PET) allows us to measure regional cerebral glucose metabolism semi-quantitatively and to visualize the distribution of altered glucose metabolism [3–5]. In most patients with TLE, interictal FDG-PET shows hypometabolism in the temporal lobe harboring the epileptogenic focus. While the mechanisms underlying metabolic dysfunction have not been elucidated, it is considered to be closely related to epileptogenicity [6–8]. Therefore, the cerebral metabolism distribution on preoperative FDG-PET may differ between the patients with seizure-free outcomes and those with non-seizure-free outcomes after TLE surgery.

Previous studies with FDG-PET showed the presence of hypometabolism in the unilateral temporal lobe ipsilateral to the surgical site to be predictive of a good seizure outcome, and that widespread hypometabolism beyond the temporal lobe is associated with a poor outcome [9–12]. However, hypometabolism is frequently extensive in TLE patients [13]. It is thus necessary to characterize the involvement of the extra-temporal area as well as that of the temporal lobe. However, there is some difficulty in objective evaluation of metabolic changes in the extra-temporal area, because the changes are frequently mild, though they can be detected visually [14].

In this study, we aimed to elucidate the differences in glucose hypometabolism on preoperative interictal FDG-PET between patients with and without seizure-free outcomes. To investigate differences including mild hypometabolism, we applied a voxel-based Asymmetry index (AI) method, in which each voxel value was calculated as the AI instead of using an adjustment method with the cerebral global mean. The AI of hypometabolism is an important index especially for evaluating unilateral hemispheric disease. Some studies have applied AI for the evaluation of hypometabolism; the AI was calculated using the mean count of the ipsilateral and contralateral region of interest (ROI) [11, 15, 16]. Instead of using the mean of the ROI, we calculated the AI for each voxel. Furthermore, we employed two types of analysis. One was voxel severity analysis, which is a widely used method of comparing voxel values at the same coordinate, and the other was extent analysis, in which we counted the number of voxels exceeding a threshold in the predefined volume of interest (VOI) and compared the number of voxels between the two patient groups. We previously reported the combination of this voxel-based AI method and extent analysis to improve the accuracy of epileptogenic zone localization [17]. Therefore, using this method as well as conventional analysis, we attempted to evaluate cerebral cortical hypometabolism.

Materials and methods

Patients and controls

We identified all patients ($n = 145$) who underwent interictal FDG-PET for epilepsy evaluation between 2003 and 2009. Among these patients, 51 were clinically diagnosed as unilateral mesial temporal lobe epilepsy (mTLE) and received surgical treatment of the unilateral hippocampal area, and we selected 28 of these patients (15 males and 13 females, mean age 34.5 ± 9.7 years) for this study based on the following inclusion criteria: (1) followed up for at least 2 years after surgery; (2) preoperative evaluations including interictal electroencephalography (EEG), interictal and ictal scalp/sphenoidal video-EEG recording, magnetic resonance imaging (MRI), interictal cerebral perfusion single photo emission computed tomography (SPECT), iomazenil SPECT, and interictal FDG-PET had been performed; (3) no space occupying lesion exceeding 1 cm in diameter on MRI; (4) no history of either previous cranial surgery or encephalomyelitis. These preoperative examinations were performed as part of routine evaluations for patients who were surgical candidates for medically refractory epilepsy. Preoperative identification of the epileptogenic zone (EZ) was based on these preoperative evaluations and clinical semiology. FDG-PET was used only for the diagnosis for unilateral mTLE based on decreased FDG in the temporal lobe. Intracranial electrode evaluation was also performed when the concordance of these preoperative evaluations was insufficient.

All patients in this study underwent surgical resection and/or transection of the unilateral hippocampal area [18]. The surgical area was extended to structures neighboring the hippocampus, as necessary. The extent of surgery was decided according to intra-surgical electrocorticography (ECoG) findings.

Patient characteristics are listed in Table 1. Postoperative seizure outcome was evaluated according to the Engel's classification [19] by reviewing medical records. In all analyses, patients were divided into two groups: (1) seizure-free (Engel class 1a and 1b) and (2) non-seizure-free (Engel class 1c and 1d, 2–4). Surgical outcomes were evaluated at 2 years after surgery, but in cases with recurrence within the 2-year follow-up period, outcomes were evaluated at the time of the recurrence. With visual evaluation for clinical diagnosis of mTLE, preoperative FDG-PET showed obvious decrease in the ipsilateral temporal lobe in 20 patients, in other 8 patients, decreases were unobvious or bilateral. There were no significant differences between the seizure-free and non-seizure-free groups in clinical factors, age at onset, epilepsy duration, age at surgery, seizure frequency, surgical side or temporal lobe decreases on preoperative FDG-PET by visual

Table 1 Patient characteristics

	SZ-free (n = 17)	Non SZ-free (n = 11)	p value
Gender			N.S.
Male	9	6	
Female	8	5	
Age at onset (year)	12.3 ± 10.6	12.0 ± 6.5	N.S.
Duration of epilepsy (year)	23.0 ± 11.8	22.3 ± 9.4	N.S.
Age at surgery (year)	35.3 ± 10.5	32.9 ± 8.5	N.S.
Seizure frequency (number of patients)			N.S.
Daily	6	2	
Weekly	6	2	
Monthly	4	7	
Side of surgery			N.S.
Right	2	5	
Left	15	6	
Visual evaluation of preoperative FDG-PET ^a			N.S.
Ipsi TL decrease	13	7	
Not diagnostic	4	4	

SZ-free seizure-free group, N.S. not significant

^a With visual evaluation for clinical diagnosis of mTLE, “Ipsi TL decrease” means obvious decrease in the ipsilateral temporal lobe on preoperative FDG-PET, and “Not diagnostic” means that the decreases were unobvious or found in the bilateral temporal lobes

evaluation (Fisher’s exact test at a significance level of 5 %). Of the 28 patients in this study, 11 were classified into the non-seizure-free group, but most patients had benefitted from surgical therapy. Two patients required a second surgery within the 2-year follow-up period.

FDG-PET scans of the controls were obtained employing an identical protocol for 20 normal controls, as in our previous study [17]. The controls were 11 males and 9 females. Their mean age was 47, range 24–60 years. None had neurological or mental diseases, or any history of cranial surgery or anti-psychotic drug use.

This retrospective study was performed according to the guidelines of the Ethics Review Board of Tokyo University Hospital. Written informed consent was obtained from all patients and controls. We also obtained permission to analyze the clinical data.

FDG-PET acquisition

The patients fasted for at least 5 h and then underwent FDG-PET scanning. A 296 MBq (8 mCi) dose of FDG was injected intravenously, and 45 min later, emission scans were obtained in two-dimensional mode for 10 min, and transmission scans were subsequently obtained to correct for photon attenuation using a ⁶⁸Ga/⁶⁸Ge rotating rod source. The PET scanner was an Advance NXi (General Electric

Medical Systems), with 12096 bismuth-germinate crystals arranged in 18 rings and a 15.2 cm axial field-of-view. The scanner has an intrinsic spatial resolution in the center of the field-of-view of 4.8 mm full width of half maximum (FWHM) and an axial resolution of 4.0 mm FWHM.

During the examination, in a quiet room, the patient rested in the supine position with an eye mask to minimize the confounding factor of environmental noises, and was observed for exclusion of clinical seizure activity. During the scan, the patient’s head was kept in the head holder, and when the head moved, a radiology technician corrected the movement according to a mark on the patient’s head and a laser pointer device. The FDG-PET data were reconstructed with ordered subset expectation maximization iterative reconstruction, with 2 iterations and 28 subsets. An 8-mm FWHM Gaussian filter was applied to the image. The data were collected for 37 transaxial slices of a 128 × 128 matrix, with a pixel size of 2.03 × 2.03 mm, and 35 successive slices were separated by 4.25 mm.

¹⁸F was synthesized using the Cypris Model 370 Cyclotron (Sumitomo Heavy Industries), and FDG was generated with an automated FDG synthesis system (F100: Sumitomo Heavy Industries) on the day of each scan. Radiochemical purity was greater than 95 %.

FDG-PET image processing and statistical analysis

Data analysis was performed using SPM8 and MATLAB version R2011a (MathWorks Inc., Natick, MA, USA). The data analysis steps were: (1) spatial normalization; (2) smoothing; (3) right–left flipping of the images of patients with left TLE; (4) voxel-value adjustment with GN and AI; (5) z score mapping for extent analysis; (6) statistical comparison with voxel severity analysis and (7) extent analysis. This study included patients with right mTLE and patients with left mTLE. The surgical side was set as the right side of the hemisphere, and is described as “ipsilateral” throughout this study.

Processes from (1) to (5) were described in detail in our previous study [17]. In brief, (1) all FDG-PET images (28 mTLE patients and 20 controls) were spatially normalized and (2) smoothed. (3) The images of left mTLE patients were flipped so as to place the affected temporal lobe on the right side in all patients. (4) Voxel values were adjusted by two methods. One was dividing voxel values by the mean value of the whole brain [20]. The other was calculating AI for each voxel. AI images were calculated with non-flipped and flipped images of normalized control and patient images using:

$$V_{AI} = (V_{nf} - V_f) / (V_{nf} + V_f), \quad (1)$$

where V_{AI} represents the AI image, V_{nf} is the non-flipped image, and V_f is the flipped image. AI images were

smoothed using a three-dimensional isotropic Gaussian kernel with a FWHM of 4 mm. (5) For extent analysis, the resulting images were mapped using z scores, calculated on a voxel-by-voxel basis using:

$$Z = (V_m - V_p) / SD, \quad (2)$$

where Z represents the z score, V_m the mean of the corresponding control voxel values, V_p the patient's corresponding voxel values, and SD the standard deviation of the corresponding control voxel values. (6) Voxel severity analysis; to compare the severity of the voxel values of each group (voxel severity analysis), voxel-by-voxel comparison at the same coordinate was performed between the seizure-free group and controls, the non-seizure-free group and controls, and the seizure-free and non-seizure-free groups. Statistical comparisons were performed by t test with SPM. We investigated hypometabolic areas at a height threshold of $p < 0.05$ with family-wise error (FWE) correction for multiple comparisons and an extent threshold of 100 voxels. If no significant voxels were detected, the height threshold was relaxed to $p < 0.001$ (uncorrected). (7) extent analysis; symmetrical right- and left-VOIs were defined by overlapping areas of the right- and left-sided VOIs of the Talairach Deamon Atlas (level 3) [21, 22]. The Talairach Deamon Atlas (level 3) originally showed 55 VOIs on each side. These VOIs were grouped into 7 anatomic areas, including the frontal area, hippocampal area, lateral temporal area, parietal area, occipital area, basal ganglia, and thalamic area on each side, and

were converted into the MNI space. Then, we calculated the percentage of the number of voxels exceeding a threshold set at z equal to 0.5, 1.0, 1.5 or 2.0, in these anatomical areas. To compare the extent of hypometabolism of each VOI between the seizure-free and non-seizure-free groups, the Mann–Whitney test was performed. The level of statistical significance was set at a two-sided p value < 0.05 . The flow chart of data analysis of voxel severity analysis (6) and extent analysis (7) is depicted in Fig. 1.

Statistical analyses except for the voxel severity analysis were performed using SPSS for Windows (version 16; SPSS Inc, Chicago, IL, USA).

Results

Voxel severity analysis

In comparison with controls, the seizure-free group showed a significant decrease in the ipsilateral temporal pole with the GN method ($p < 0.05$, FWE corrected) (Fig. 2), and in the ipsilateral mesial temporal area and temporal pole with the AI method ($p < 0.05$, FWE corrected) (Fig. 3). The voxel peak in these significant areas is listed with the Talairach coordinate, T value, cluster size and anatomical region on Talairach's atlas in Table 2. In the non-seizure-free group as compared with the controls, no significant decrease was detected with the stringent threshold

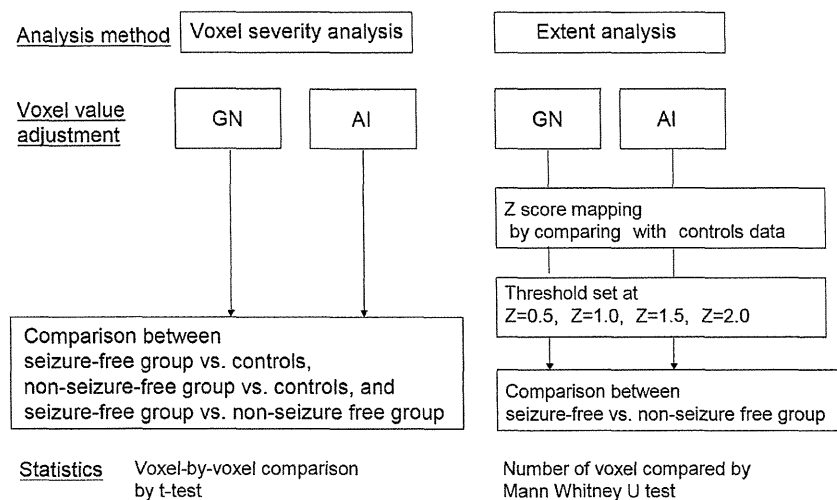


Fig. 1 The flow chart of data analysis depicts two types of statistical analysis; voxel severity and extent analyses. With regards to the voxel-value adjustment, the GN method and the AI method were applied. In the voxel severity analysis, comparison between the seizure-free group and controls, the non-seizure-free group and controls, and the seizure-free and non-seizure-free groups were

performed with adjustment for each voxel-value. In the extent analysis, the voxel value was converted to the z score based on control data. Extent was calculated by counting the number of voxels exceeding the predefined threshold. We tried 4 thresholds with z scores ranging from 0.5 to 2.0. Then, the extents of anatomical areas were compared between the seizure-free and non-seizure-free groups

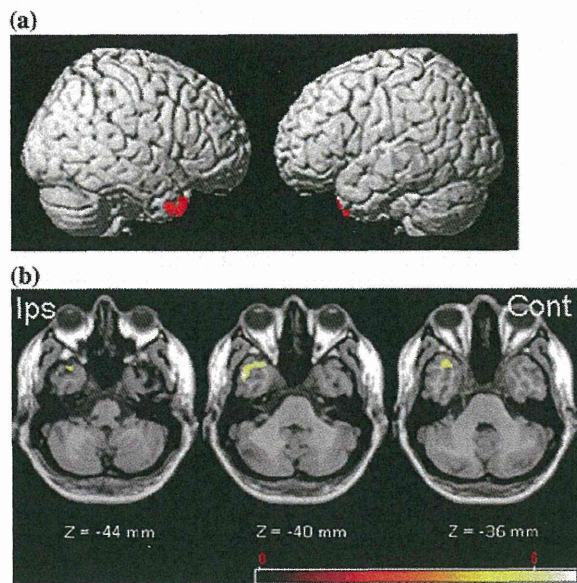


Fig. 2 Comparison between seizure-free group and controls by the GN method ($p < 0.05$ FWE corrected, voxel size > 100). **a** Surface view, **b** axial images of areas with significant decreases. Colored bar represents t value. *Ips* ipsilateral to the surgical side, *Cont* contralateral to the surgical side. The region in color represents the significantly decreased area in the seizure-free group as compared to the controls. The surgical side was set as the right side in this display

($p < 0.05$, FWE corrected) (Figure not shown). With the lenient threshold ($p < 0.001$, uncorrected), a part of the contralateral frontal gyrus, ipsilateral insular area and ipsilateral temporal lobe was detected with AI, but not with GN (Table 3).

Comparison between the seizure-free and non-seizure-free groups revealed no significant voxels detectable with the stringent threshold ($p < 0.05$, FWE corrected). Significant voxels detected with the lenient threshold ($p < 0.001$, uncorrected) are listed in Table 4. The seizure-free group showed a significant decrease in the posterior part of the ipsilateral lentiform nucleus with both the GN and the AI method. On the other hand, when the non-seizure-free group was compared with the seizure-free group, no significantly decreased voxels were detected with the GN method. With the AI method, a significant decrease was detected in the contralateral lentiform nucleus, which is the only contralateral coordinate showing a significant decrease in the seizure-free group as compared to the non-seizure-free group, because the absolute value of AI is equal on the left and right sides at the same coordinate.

Extent analysis

With the AI method and the voxel threshold at $z = 1$, a significant difference was detected in regions of the ipsilateral

hippocampal ($p = 0.01$), ipsilateral frontal ($p = 0.03$), ipsilateral thalamic ($p = 0.01$), contralateral frontal ($p = 0.01$) and contralateral thalamic ($p = 0.01$) areas between the seizure-free and non-seizure-free groups. In these areas of the ipsilateral hemisphere, the extent of hypometabolism was larger in the seizure-free than in the non-seizure-free group. On the other hand, in the contralateral frontal area and the thalamus, the extent was smaller in the seizure-free than in the non-seizure-free group. With the AI method and the voxel threshold at $z = 0.5$, a significant difference was detected in the same areas. With the other combinations of the z threshold and the voxel value adjustment method, a significant difference was detected in parts of these areas. With a threshold of $z = 2.0$, only the ipsilateral thalamus showed a significant difference using the GN method ($p = 0.03$) and the AI method ($p = 0.02$). Significantly different areas, median extents and the p values determined with the z threshold using the GN method are listed in Table 5, and those obtained using the AI method in Table 6.

Discussion

We detected differences in the distribution of preoperative cerebral hypometabolism between patients who obtained seizure-free outcomes and those who were not seizure free after surgery. The differences were detected in the bilateral frontal lobe, thalamus, lentiform nucleus and ipsilateral temporal lobe. Our results suggest ipsilateral dominance of hypometabolism in the frontal lobe and subcortical areas, and severe hypometabolism restricted to the ipsilateral temporal lobe to be associated with seizure-free outcomes after unilateral TLE surgery.

In comparison with the controls, the severe hypometabolism detected by voxel severity analysis with the stringent threshold was restricted to the temporal lobe on the surgical side in the group of patients with seizure-free outcomes, which agrees with previous reports [9–12]. In contrast, no significant decreases were detected in the non-seizure-free group. This suggests that the hypometabolism of patients in the non-seizure-free group was less restricted to the unilateral temporal lobe and did not show common features among patients. When using the AI method with the lenient threshold in voxel severity analysis, decreased areas were detected in some areas of the ipsilateral temporal lobe, the ipsilateral insular area, and the contralateral frontal lobe in the non-seizure-free group. These decreases in the ipsilateral temporal lobe and the insular area are considered to be closely related to TLE, because all patients in this study benefitted from surgical therapy involving the unilateral temporal lobe and neighboring structures.

With regard to the extra-temporal lobe area, extent analysis with the AI method was most sensitive for

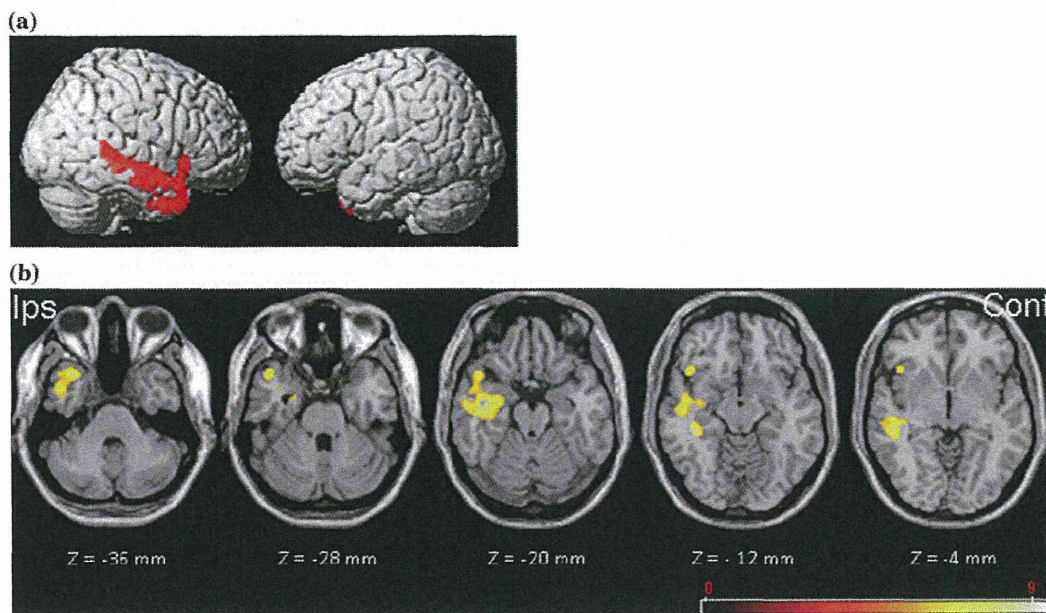


Fig. 3 Comparison between seizure-free group and controls with the AI method ($p < 0.05$ FWE corrected, voxel size > 100). **a** Surface view, **b** axial images of areas with significant decreases. *Colored bar* represents *t* value. *Ips* ipsilateral to the surgical side, *Cont*

contralateral to the surgical side. The region in *color* represents the significantly decreased area in the seizure-free group as compared to the controls. The surgical side was set as the right side in this display

Table 2 Voxel peak in significant area detected by severity voxel analysis in the comparison between the seizure-free group and controls ($p < 0.05$, FWE corrected)

	Coordinates			<i>T</i> value	Cluster size	Cerebral regions on Talairach atlas
	<i>X</i>	<i>Y</i>	<i>Z</i>			
GN method	44	9	-30	6.88	128	Ipsilateral superior temporal gyrus
AI method	45	-37	1	9.43	2039	Ipsilateral superior temporal gyrus

Table 3 Voxel peak in significant area detected by the severity voxel analysis in the comparison between the non-seizure-free group and controls ($p < 0.001$, uncorrected)

	Coordinates			<i>T</i> value	Cluster size	Cerebral regions on Talairach atlas
	<i>X</i>	<i>Y</i>	<i>Z</i>			
GN method	N.S.					
AI method	-42	40	25	6.48	172	Contralateral middle frontal gyrus
	35	13	-34	5.06	136	Ipsilateral superior temporal gyrus
	42	17	-1	5.03	133	Ipsilateral insula
	52	-42	8	4.87	517	Ipsilateral middle temporal gyrus

N.S. not significant

detecting differences between the two patient groups. We consider voxel-based AI to facilitate detection of mild hypometabolism because AI is a sensitive index, especially for hemispheric disease. Furthermore, AI calculation using the voxel-by-voxel approach probably overcomes the disadvantages of VOI-based AI, such as the VOI-dependent

fluctuation of AI values and the underestimation caused by the “averaging effect” [23]. The combination with extent analysis allows us to compare the number of voxels exceeding a threshold, even if the threshold is low, corresponding to mild hypometabolism. Also, this method is probably similar to visual evaluation. We usually conduct

Table 4 Voxel peak in significant area detected by the severity voxel analysis in the comparison between the seizure-free and non-seizure-free groups ($p < 0.001$, uncorrected)

Comparison pair and Method	Coordinates			<i>T</i> value	Cluster size	Cerebral regions on Talairach atlas
	<i>X</i>	<i>Y</i>	<i>Z</i>			
<i>SZ-free</i> < Non- <i>SZ-free</i>						
GN method	32	−21	5	4.99	138	Ipsilateral lentiform nucleus
AI method	29	−17	8	5.08	177	Ipsilateral lentiform nucleus
Non <i>SZ-free</i> < <i>SZ-free</i>						
GN method	N.S.					
AI method	−29	−17	8	5.08	177	Contralateral lentiform nucleus ^a

SZ-free seizure-free group

^a Symmetrical region detected by comparison between seizure-free and non-seizure-free groups performed with AI, because the absolute voxel value is symmetrical

Table 5 Anatomical areas showing significant difference between seizure-free group and non-seizure-free group in analysis with the combination of the GN method and the extent analysis

Threshold	Anatomical area	Median extent (%) ^a		<i>p</i> value
		Seizure-free group	Non-seizure-free group	
<i>z</i> = 0.5	Ipsilateral hippocampal area	61.5	37.1	0.01
<i>z</i> = 1.0	Ipsilateral hippocampal area	44.6	23.7	0.04
<i>z</i> = 1.5	Ipsilateral hippocampal area	29.7	14.1	0.04
	Ipsilateral thalamic area	32.5	9.9	0.02
<i>z</i> = 2.0	Ipsilateral thalamic area	22.4	3.7	0.03

^a Median extent (%); Extent (%) is the percentage of the number of voxels exceeding *z* threshold set at *z* = 0.5, 1.0, 1.5, or 2.0, respectively, in the anatomical areas. Median extent (%) is a median value of the extent (%) in each group

Table 6 Anatomical areas showing significant difference between seizure-free group and non-seizure-free group in analysis with the combination of the AI method and the extent analysis

Threshold	Anatomical area	Median extent (%) ^a		<i>p</i> value
		Seizure-free group	Non-seizure-free group	
<i>z</i> = 0.5	Ipsilateral hippocampal area	70.3	46.5	0.01
	Ipsilateral frontal area	52.6	37.7	0.02
	Ipsilateral thalamic area	58.0	26.9	0.02
	Contralateral frontal area	17.6	28.6	0.03
	Contralateral thalamic area	15.8	37.8	<0.01
<i>z</i> = 1.0	Ipsilateral hippocampal area	58.0	30.3	0.01
	Ipsilateral frontal area	36.5	22.7	0.03
	Ipsilateral thalamic area	46.7	14.6	0.01
	Contralateral frontal area	8.5	16.3	0.01
	Contralateral thalamic area	7.4	20.1	0.01
<i>z</i> = 1.5	Ipsilateral hippocampal area	45.3	19.3	0.02
	Ipsilateral thalamic area	37.3	7.2	0.01
	Contralateral frontal area	3.9	8.5	0.03
	Contralateral thalamic area	3.3	9.1	0.01
<i>z</i> = 2.0	Ipsilateral thalamic area	30.0	3.4	0.02

^a Median extent (%); Extent (%) is the percentage of the number of voxels exceeding *z* threshold set at *z* = 0.5, 1.0, 1.5, or 2.0 respectively in the anatomical areas. Median extent (%) is a median value of the extent (%) in each group

visual evaluation primarily in consideration of inter-hemispheric asymmetry and the extent of the asymmetry of each region.

When we used the AI method in extent analysis with a low threshold of $z = 0.5$ or 1.0 , the differences were detected in the bilateral frontal lobe and thalamus. With a high threshold of $z = 2.0$, a significant difference was detected only in the ipsilateral thalamus. This may imply that the extent of hypometabolism including mild changes differs between the frontal lobe and the thalamus, and that the extent of relatively severe hypometabolism differs only in the thalamus between the two patient groups. In these areas, contralateral dominance of hypometabolism was observed in the non-seizure-free group, which is consistent with a previous report describing reverse thalamic metabolic asymmetry in patients with poor outcomes [15].

Ipsilateral dominant hypometabolism in the thalamus is frequently observed in patients with TLE [13, 24]. Other studies using ictal perfusion SPECT also showed significant hyperperfusion in the ipsilateral putamen and thalamus as well as the temporal lobe [25]. The degree of thalamic hypometabolism in TLE was associated with a longer duration of epilepsy and a history of secondary generalized convulsions [26]. An animal study also demonstrated persistent hypometabolism in the hippocampus and thalamus in the chronic phase [27]. Based on animal studies, Gale [28] suggested that the thalamus has a reciprocal connection with all limbic structures, which contain a population of neurons vulnerable to irritative activity and also the first to evoke epileptic seizures by stimulation of various forebrain sites. It seems likely that the thalamus is involved in the pathway of transmission of seizure activity. Thalamic hypometabolism may correlate with metabolic dysfunction of the limbic system through dense connections and it may also reflect diffuse hypometabolism of cerebral cortices collectively.

Ipsilateral frontal hypometabolism reportedly has a close relationship with TLE. Comparing ictal perfusion SPECT with interictal FDG-PET, concordance of abnormalities of ictal hyperperfusion and hypometabolism was detected predominantly on the ipsilateral orbitofrontal and insular cortex [29]. In addition, the ipsilateral orbitofrontal area showed hyperperfusion during the initial phase of the seizure, shifting to hypoperfusion in a later phase, suggesting the propagation of epileptic activity followed by surround inhibition [25]. In this study, we also demonstrated a correlation between the extent of hypometabolism in the ipsilateral frontal lobe and those of the ipsilateral hippocampal area in seizure-free outcome patients ($R = 0.52$, $p = 0.02$, Spearman rank correlation test). In contrast, this correlation was not detected in non-seizure-free outcome patients. Therefore, ipsilateral frontal hypometabolism may support the existence of an EZ in the

ipsilateral temporal area. However, the interpretation of frontal hypometabolism requires caution, because depression and cognitive impairment, which are frequently associated with TLE, also show frontal hypometabolism [30–32]. The consistency of the laterality of predominant hypometabolism between the temporal and frontal lobes may facilitate distinguishing whether hypometabolism is closely related to TLE itself or a secondary cognitive dysfunction due to epilepsy.

All patients in this study were preoperatively diagnosed as having mTLE based on comprehensive examinations and semiology. Electrical abnormalities with intra-surgical ECoG were detected in the hippocampal area of the surgical side, and the extent of surgery for the temporal area and surrounding structures was decided based on the ECoG findings. If the EZ exists far from the surgical field, which cannot be investigated by ECoG, then, surgical intervention cannot be performed, and seizure control may therefore be less likely to be obtained. Our non-seizure-free patients showed contralateral dominant hypometabolism in the frontal lobe and thalamus, which suggests that the metabolic dysfunction related to epileptogenesis may not be limited to the area around the ipsilateral temporal lobe.

We have to mention about the limitation of image analysis applying asymmetry index. Asymmetry index cannot differentiate between the ipsilateral hypometabolism and the contralateral hypermetabolism. Van Bogaert et al. reported that the contralateral temporal hypermetabolism was detected in patients with unilateral mTLE with voxel-based statistical analysis. They interpreted it as reflecting compensatory mechanisms, but also gave a caution of the possibility of subclinical epileptic activity [33]. In this study, we visually evaluated the preoperative FDG-PET images for diagnosis of mTLE, and did not detect any focal increased area with suspected epileptic discharge. In addition, GN method as well as AI method was applied, and there was no contradictive results between the two methods, but we cannot exclude the possibility of the slight contralateral hypermetabolism contributing to improve the sensitivity of AI method.

The results of this study confounded neither the surgical method and nor the surgical area. The hypometabolism in the temporal lobe was used only for the diagnosis of mTLE. In the future study, multiple regression analysis should be performed to assess the influences of our observations and other factors including MRI results, intra-surgical ECoG findings and surgical method in a large number of patients.

In conclusion, differences in the distribution of preoperative hypometabolism between patients with and without seizure-free outcomes were detected with voxel-based statistical analysis. Differences were detected in the frontal lobe and the subcortical area as well as the temporal lobe. The ipsilateral predominant hypometabolism including mild changes in the

frontal lobe and thalamus may support epileptogenesis being limited to the ipsilateral temporal lobe and surrounding area. Not only whether hypometabolism is restricted to the temporal lobe, but also the laterality of hypometabolism in the frontal lobe and the thalamus may facilitate predicting seizure outcomes after unilateral TLE surgery.

Acknowledgments We would like to thank the staff of our Nuclear Medicine Department and our secretaries, for their contributions to this study.

References

1. Wiebe S, Blume WT, Girvin JP, Eliasziw M. A randomized, controlled trial of surgery for temporal-lobe epilepsy. *N Engl J Med*. 2001;345:311–8.
2. Salanova V, Markand O, Worth R. Longitudinal follow-up in 145 patients with medically refractory temporal lobe epilepsy treated surgically between 1984 and 1995. *Epilepsia*. 1999;40:1417–23.
3. Sokoloff L, Reivich M, Kennedy C, Des Rosiers MH, Patlak CS, Pettigrew KD, et al. The [¹⁴C]deoxyglucose method for the measurement of local cerebral glucose utilization: theory, procedure, and normal values in the conscious and anesthetized albino rat. *J Neurochem*. 1977;28:897–916.
4. Reivich M, Kuhl D, Wolf A, Greenberg J, Phelps M, Ido T, et al. The [¹⁸F]fluorodeoxyglucose method for the measurement of local cerebral glucose utilization in man. *Circ Res*. 1979;44:127–37.
5. Alavi A, Dann R, Chawluk J, Alavi J, Kushner M, Reivich M. Positron emission tomography imaging of regional cerebral glucose metabolism. *Semin Nucl Med*. 1986;16:2–34.
6. Henry TR, Babb TL, Engel J Jr, Mazziotta JC, Phelps ME, Crandall PH. Hippocampal neuronal loss and regional hypometabolism in temporal lobe epilepsy. *Ann Neurol*. 1994;36:925–7.
7. Vinton AB, Carne R, Hicks RJ, Desmond PM, Kilpatrick C, Kaye AH, et al. The extent of resection of FDG-PET hypometabolism relates to outcome of temporal lobectomy. *Brain*. 2007;130:548–60.
8. Matheja P, Kuwert T, Ludemann P, Weckesser M, Kellinghaus C, Schuierer G, et al. Temporal hypometabolism at the onset of cryptogenic temporal lobe epilepsy. *Eur J Nucl Med*. 2001;28:625–32.
9. Radtke RA, Hanson MW, Hoffman JM, Crain BJ, Walczak TS, Lewis DV, et al. Temporal lobe hypometabolism on PET: predictor of seizure control after temporal lobectomy. *Neurology*. 1993;43:1088–92.
10. Manno EM, Sperling MR, Ding X, Jaggi J, Alavi A, O'Connor MJ, et al. Predictors of outcome after anterior temporal lobectomy: positron emission tomography. *Neurology*. 1994;44:2331–6.
11. Theodore WH, Sato S, Kufta CV, Gaillard WD, Kelley K. FDG-positron emission tomography and invasive EEG: seizure focus detection and surgical outcome. *Epilepsia*. 1997;38:81–6.
12. Choi JY, Kim SJ, Hong SB, Seo DW, Hong SC, Kim BT, et al. Extratemporal hypometabolism on FDG PET in temporal lobe epilepsy as a predictor of seizure outcome after temporal lobectomy. *Eur J Nucl Med Mol Imaging*. 2003;30:581–7.
13. Henry TR, Mazziotta JC, Engel J Jr. Interictal metabolic anatomy of mesial temporal lobe epilepsy. *Arch Neurol*. 1993;50:582–9.
14. Hashiguchi K, Morioka T, Yoshida F, Kawamura T, Miyagi Y, Kuwabara Y, et al. Thalamic hypometabolism on 18FDG-positron emission tomography in medial temporal lobe epilepsy. *Neurol Res*. 2007;29:215–22.
15. Newberg AB, Alavi A, Berlin J, Mozley PD, O'Connor M, Sperling M. Ipsilateral and contralateral thalamic hypometabolism as a predictor of outcome after temporal lobectomy for seizures. *J Nucl Med*. 2000;41:1964–8.
16. Lee SK, Lee DS, Yeo JS, Lee JS, Kim YK, Jang MJ, et al. FDG-PET images quantified by probabilistic atlas of brain and surgical prognosis of temporal lobe epilepsy. *Epilepsia*. 2002;43:1032–8.
17. Soma T, Momose T, Takahashi M, Koyama K, Kawai K, Murase K, et al. Usefulness of extent analysis for statistical parametric mapping with asymmetry index using inter-ictal FGD-PET in mesial temporal lobe epilepsy. *Ann Nucl Med*. 2012;26:319–26.
18. Shimizu H, Kawai K, Sunaga S, Sugano H, Yamada T. Hippocampal transection for treatment of left temporal lobe epilepsy with preservation of verbal memory. *J Clin Neurosci*. 2006;13:322–8.
19. Engel J Jr, Van Ness PC, Rasmussen TB, Ojemann LM. Outcome with respect to epileptic seizures. In: Engel Jr J, editor. *Surgical treatment of the epilepsies*. New York: Raven Press; 1993. p. 609–21.
20. Fox PT, Mintun MA, Reiman EM, Raichle ME. Enhanced detection of focal brain responses using intersubject averaging and change-distribution analysis of subtracted PET images. *J Cereb Blood Flow Metab*. 1988;8:642–53.
21. Lancaster JL, Rainey LH, Summerlin JL, Freitas CS, Fox PT, Evans AC, et al. Automated labeling of the human brain: a preliminary report on the development and evaluation of a forward-transform method. *Hum Brain Mapp*. 1997;5:238–42.
22. Lancaster JL, Woldorff MG, Parsons LM, Liotti M, Freitas CS, Rainey L, et al. Automated Talairach atlas labels for functional brain mapping. *Hum Brain Mapp*. 2000;10:120–31.
23. Rubin E, Dhawan V, Moeller JR, Takikawa S, Labar DR, Schaul N, et al. Cerebral metabolic topography in unilateral temporal lobe epilepsy. *Neurology*. 1995;45:2212–23.
24. Khan N, Leenders KL, Hajek M, Maguire P, Missimer J, Wieser HG. Thalamic glucose metabolism in temporal lobe epilepsy measured with 18F-FDG positron emission tomography (PET). *Epilepsy Res*. 1997;28:233–43.
25. Dupont P, Zaknun JJ, Maes A, Tepmongkol S, Vasquez S, Bal CS, et al. Dynamic perfusion patterns in temporal lobe epilepsy. *Eur J Nucl Med Mol Imaging*. 2009;36:823–30.
26. Benedek K, Juhasz C, Muzik O, Chugani DC, Chugani HT. Metabolic changes of subcortical structures in intractable focal epilepsy. *Epilepsia*. 2004;45:1100–5.
27. Guo Y, Gao F, Wang S, Ding Y, Zhang H, Wang J, et al. In vivo mapping of temporospatial changes in glucose utilization in rat brain during epileptogenesis: an 18F-fluorodeoxyglucose-small animal positron emission tomography study. *Neuroscience*. 2009;162:972–9.
28. Gale K. Subcortical structures and pathways involved in convulsive seizure generation. *J Clin Neurophysiol*. 1992;9:264–77.
29. Bouilleret V, Boyet S, Marescaux C, Nehlig A. Mapping of the progressive metabolic changes occurring during the development of hippocampal sclerosis in a model of mesial temporal lobe epilepsy. *Brain Res*. 2000;852:255–62.
30. Lambert MV, Robertson MM. Depression in epilepsy: etiology, phenomenology, and treatment. *Epilepsia*. 1999;40:S21–47.
31. Hosokawa T, Momose T, Kasai K. Brain glucose metabolism difference between bipolar and unipolar mood disorders in depressed and euthymic states. *Prog Neuropsychopharmacol Biol Psychiatry*. 2009;33:243–50.
32. Takaya S, Hanakawa T, Hashikawa K, Ikeda A, Sawamoto N, Nagamine T, et al. Prefrontal hypofunction in patients with intractable mesial temporal lobe epilepsy. *Neurology*. 2006;67:1674–6.
33. Van Bogaert P, Massager N, Tugendhaft P, Wikler D, Damhaut P, Levisier M, et al. Statistical parametric mapping of regional glucose metabolism in mesial temporal lobe epilepsy. *Neuroimage*. 2000;12:129–38.

Usefulness of extent analysis for statistical parametric mapping with asymmetry index using inter-ictal FDG-PET in mesial temporal lobe epilepsy

Tsutomu Soma · Toshimitsu Momose ·
Miwako Takahashi · Keittraro Koyama ·
Kensuke Kawai · Kenya Murase · Kuni Ohtomo

Received: 19 October 2011 / Accepted: 15 January 2012 / Published online: 8 February 2012
© The Japanese Society of Nuclear Medicine 2012

Abstract

Objective Inter-ictal ^{18}F -2-fluoro-deoxy-D-glucose-positron emission tomography (FDG-PET) is widely used for preoperative evaluation to identify epileptogenic zones in patients with temporal lobe epilepsy. In this study, we combined statistical parametric mapping (SPM) with the asymmetry index and volume-of-interest (VOI) based extent analysis employing preoperative FDG-PET in unilateral mesial temporal lobe epilepsy (MTLE) patients. We also evaluated the detection utility of these techniques for automated identification of abnormalities in the unilateral hippocampal area later confirmed to be epileptogenic zones by surgical treatment and subsequent good seizure control.

Methods FDG-PET scans of 17 patients (9 males, mean age 35 years, age range 16–60 years) were retrospectively

analyzed. All patients had been preoperatively diagnosed with unilateral MTLE. The surgical outcomes of all patients were Engel class 1A or 1B with postoperative follow-up of 2 years. FDG-PET images were spatially normalized and smoothed. After two voxel-value adjustments, one employing the asymmetry index and the other global normalization, had been applied to the images separately, voxel-based statistical comparisons were performed with 20 controls. Peak analysis and extent analysis in the VOI in the parahippocampal gyrus were conducted for SPM. For the extent analysis, a receiver operating characteristic (ROC) curve was devised to calculate the area under the curve and to determine the optimal threshold of extent.

Results The accuracy of the method employing the asymmetry index was better than that of the global normalization method for both the peak and the extent analysis. The ROC analysis results, for the extent analysis, yielded an area under the curve of 0.971, such that the accuracy and optimal extent threshold of judgment were 92 and 32.9%, respectively.

Conclusion Statistical z-score mapping with the asymmetry index was more sensitive for detecting regional glucose hypometabolism and more accurate for identifying the side harboring the epileptogenic zone using inter-ictal FDG-PET in unilateral MTLE than z-score mapping with global normalization. Moreover, the automated determination of the side with the epileptogenic zone in unilateral MTLE showed improved accuracy when the combination of SPM with the asymmetry index and extent analysis was applied based on the VOI in the parahippocampal gyrus.

Keywords Asymmetry index · Statistical parametric mapping · FDG-PET · Mesial temporal lobe epilepsy

T. Soma · T. Momose (✉) · M. Takahashi · K. Koyama ·
K. Ohtomo
Department of Radiology, Graduate School of Medicine,
University of Tokyo, 3-1 Hongo 7-Chome, Bunkyo-ku,
Tokyo 113-8655, Japan
e-mail: tmomo-tky@umin.ac.jp

T. Soma · K. Murase
Course of Health Science, Division of Medical Technology and
Science, Department of Medical Physics and Engineering,
Graduate School of Medicine, Osaka University, Osaka, Japan

T. Soma
Software Development Group, Product Management and
Marketing Department, FUJIFILM RI Pharma Co., Ltd, Tokyo,
Japan

K. Kawai
Department of Neurosurgery, Graduate School of Medicine,
University of Tokyo, Tokyo, Japan

Introduction

Epilepsy surgery has been established as an effective treatment for patients with refractory temporal lobe epilepsy (TLE) [1, 2]. For successful surgical treatment, preoperative lateralization or localization of the epileptogenic zone (EZ) is important. Inter-ictal ^{18}F -2-fluorodeoxy-D-glucose (FDG) positron emission tomography (PET) is a widely used preoperative method of identifying the EZ. On inter-ictal FDG-PET, areas with metabolic alterations, probably related to epileptogenicity, show decreased FDG accumulation, and these findings of altered metabolism contribute to EZ detection. In preoperative evaluation with inter-ictal FDG-PET, FDG distributions are generally evaluated by visual inspection. However, visual inspection is inevitably associated with inter-observer variation and it is usually difficult to provide numerical values, such as the most appropriate threshold for diagnosis, or statistical parameters derived from comparisons with controls. Therefore, objective semi-quantitative analysis has been anticipated as a method complementing visual evaluation.

Objective semi-quantitative analysis with the region-of-interest (ROI) technique or voxel-based statistical parametric mapping [SPM; Wellcome Department of Cognitive Neurology, London, UK (<http://www.fil.ion.ucl.ac.uk/spm/>)] has been demonstrated to have utility for preoperative detection of EZ [3–6]. In addition to these methods, some studies incorporated inter-hemispheric asymmetries, such as left to right subtraction, or the asymmetry index (AI), and showed improvement of preoperative evaluations for TLE; however, in most such studies, inter-hemispheric asymmetry was calculated from the mean ROI value or the volume-of-interest (VOI) [7–9]. Few studies have applied asymmetries to voxel-based analysis. Bogaert et al. [10] prepared brain FDG-PET and mirror-reversed images of a patient, and compared them with those of normal controls by SPM. An ^{18}F -4-(2'-methoxyphenyl)-1-[2'-(*N*-2-pyridinyl)-*p*-fluorobenzamido]-ethyl-piperazine PET study demonstrated improved localization of EZ using AI calculated for each voxel, probably because the broad range of variation across normal controls was decreased using AI [11].

In this study, we calculated voxel-based AI images with FDG-PET of unilateral mesial temporal lobe epilepsy (MTLE) patients and compared them with those of normal controls, i.e., we conducted SPM employing AI. With this method, the most significant voxel in the hippocampal area on either side was identified (peak analysis). In addition, we combined the AI-SPM with VOI-based extent analysis, in which we estimated the number of voxels exceeding a threshold, because the EZ is often associated with an extensive area of hypometabolism. These methods were designed to allow automatic processing to provide

objective assessments. Then, we applied these methods to preoperative FDG-PET in patients who were candidates for epilepsy surgery, and evaluated the detection utility of these methods for identifying abnormalities in the unilateral hippocampal area later confirmed to harbor the EZ by surgical treatment and subsequent good seizure control. We also compared the diagnostic accuracy of our methods with that of the conventional global normalization (GN) method, employing SPM.

Materials and methods

Patients and controls

FDG-PET for epilepsy evaluation was performed in 145 patients between 2003 and 2009. Among these patients, 51 underwent surgical treatment of the unilateral hippocampal area, and we selected 17 of these patients (9 males, mean age 35 years, range 16–60 years) for this study based on the following inclusion criteria; (1) good postoperative outcome, corresponding to Engel's classification 1A or 1B [12] for more than 2 years; (2) preoperative evaluations including inter-ictal EEG, MRI and inter-ictal FDG-PET had been performed. All preoperative examinations were performed as part of routine evaluations for patients with medically refractory epilepsy who were candidates for epilepsy surgery. Exclusion criteria for this study were; (1) a history of previous cranial surgery, (2) space occupying lesion exceeding 1 cm on MRI; (3) a history of encephalomyelitis. We selected patients with good postoperative outcomes because the EZ was confirmed only by seizure disappearance after surgical treatment of EZ.

The control group of FDG-PET was obtained employing an identical protocol for 20 normal controls (11 males, mean age 47 years, range 24–60 years), who had no neurological or mental diseases, and no history of taking psychotropic drugs.

This retrospective study was performed according to the guidelines of the Ethical Review Board of Tokyo University Hospital. Written informed consent was obtained from all patients and controls. We also obtained permission to analyze the clinical data.

FDG-PET procedure

The patients fasted for at least 5 h and then underwent FDG-PET scanning. A 296 MBq dose of FDG was injected intravenously, and 45 min later, emission scans were obtained in two-dimensional mode for 10 min, and transmission scans were subsequently obtained to correct for photon attenuation using a $^{68}\text{Ga}/^{68}\text{Ge}$ rotating rod source.

The PET scanner was an Advance NXi (General Electric Medical Systems), with 12096 bismuth-germanate crystals arranged in 18 rings and a 15.2 cm axial field-of-view. The scanner has an intrinsic spatial resolution in the center of the field-of-view of 4.8 mm full width of half maximum (FWHM) and an axial resolution of 4.0 mm FWHM.

During the examination, the patient rested in the supine position with an eye mask to minimize the confounding factor of environmental noises, and was observed to exclude clinical seizure activity. During the scan, the patient’s head was kept in the head holder, and when the head moved, a radiology technician corrected the movement according to a mark on the patient’s head and a laser pointer device. The FDG-PET data were reconstructed with ordered subset expectation maximization iterative reconstruction, with 2 iterations and 28 subsets. An 8-mm FWHM Gaussian filter was applied to the image. The data were collected for 37 transaxial slices of a 128 × 128 matrix, with a pixel size of 2.03 × 2.03 mm, and 35 successive slices were separated by 4.25 mm.

¹⁸F was synthesized using the Cypris Model 370 Cyclotron (Sumitomo Heavy Industries), and FDG was generated with an automated FDG synthesis system (F100: Sumitomo Heavy Industries) on the day of each scan. Radiochemical purity was greater than 95%.

Data analysis

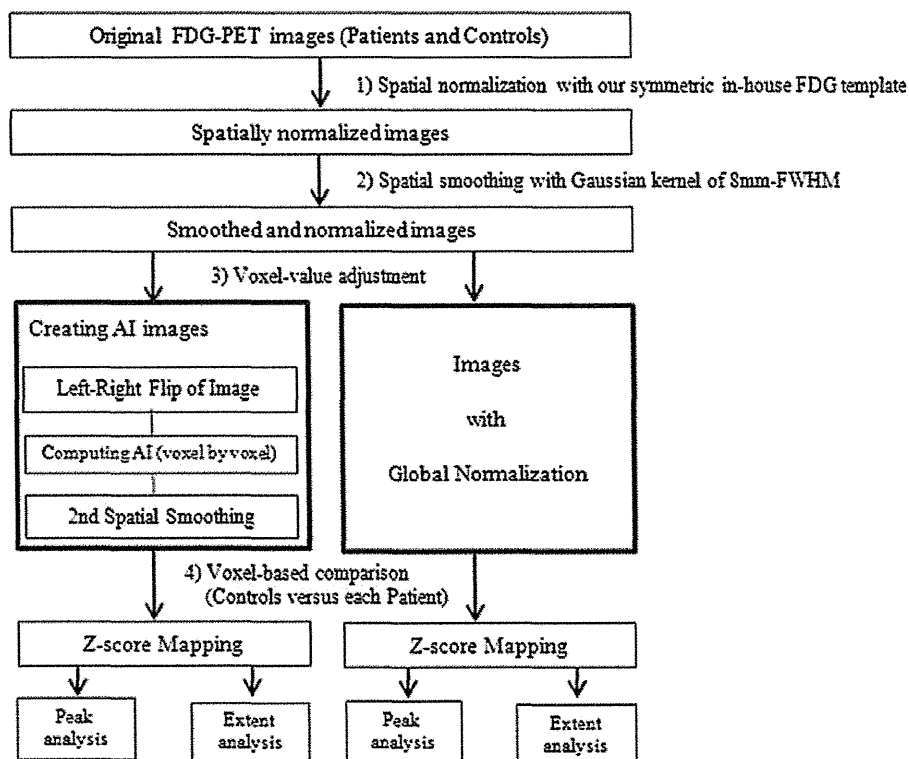
Data analysis was performed using SPM8 and MATLAB version R2011a (MathWorks Inc., Natick, MA, USA). We used MATLAB for SPM8, and to calculate a statistical value for each voxel on images pre-processed by SPM8.

The data analysis steps were: (1) spatial normalization; (2) smoothing; (3) voxel-value adjustment; (4) z-score mapping; (5) peak analysis with z-score mapping; and (6) extent analysis with z-score mapping (Fig. 1). Further details of each step are presented below.

Spatial normalization and smoothing

All FDG-PET images (17 MTLE patients and 20 controls) were spatially normalized to a standardized stereotactic Montreal Neurological Institute (MNI) space [13] based on the Talairach and Tournoux atlas [14], using 12-parameter linear affine normalization and another 16 nonlinear iteration algorithms with our in-house FDG template. The in-house FDG template was created as follows. First, the 20 control group images were spatially normalized with an FDG template which had been provided by the National Center Hospital for Mental, Nervous and Muscular Disorders [15] using the same parameter as described above. Second, the 20 normalized images were averaged, and a flipped image was

Fig. 1 The data analysis process: two types of voxel-value adjustments, the computing asymmetry index (AI) and global normalization, were performed after spatial normalization and smoothing. Then, a voxel-based comparison (z-score mapping) was performed for each type of voxel-value adjustment, followed by peak and extent analyses for each z-score map



made by reversing the mean image in the left–right direction. Third, by adding the flipped and non-flipped mean images, a symmetrical image was prepared as a semifinal template. Finally, a similar procedure was performed with the semifinal template, once again, that is, the original 20 control images were spatially normalized with the semifinal template, the 20 normalized images were averaged, a flipped image was made by reversing the mean image in the left–right direction, and the final symmetrical template was obtained by adding the flipped and non-flipped mean images.

All spatially normalized images were then smoothed using a three-dimensional isotropic Gaussian kernel with a full width at half maximum (FWHM) of 8 mm.

Voxel-value adjustment

Voxel values of normalized and smoothed images were adjusted by two methods. One method was to divide voxel values by the estimated average whole brain value of each normalized and smoothed image [16]. This method is the “global normalization with proportional scaling (GN)” generally used in SPM analysis for PET data. The other method was calculation of the AI. This method was as same as the procedure employed by Didelot and associates [11]. Each normalized and smoothed image was right and left reversed, and AI images were calculated with the non-flipped image and the corresponding flipped image using:

$$V_{AI} = (V_{nf} - V_f) / (V_{nf} + V_f) \quad (1)$$

where V_{AI} represents the AI image, V_{nf} is the non-flipped image, and V_f is the flipped image.

The second spatial smoothing was applied to each AI image using a three-dimensional isotropic Gaussian kernel with 4-mm FWHM.

Z-score mapping

Voxel-based comparisons between the patient and control groups were performed on voxel values adjusted with GN

and with AI, as described above. The resulting images for the comparisons were mapped using z scores, calculated on a voxel-by-voxel basis using:

$$Z = (V_m - V_p) / SD, \quad (2)$$

where Z represents the z score, V_m the mean of the controls' corresponding voxel values, V_p the value of the patient's corresponding voxel, and SD the standard deviation of the controls' corresponding voxel values.

VOI of parahippocampal gyrus

To decide right- and left-VOIs for the bilateral hippocampal areas, we set the parahippocampal gyrus, based on the Talairach and Tournoux atlas, at the gyrus level using Talairach Deamon [17, 18]. The area of the parahippocampal gyrus was converted into the MNI space [19] and the symmetrical VOIs were defined as the overlapping areas of the right and left sides (the left-side area was flipped over to the right and vice versa) of the parahippocampal gyrus (Fig. 2).

Peak analysis

Peak analysis was performed for each z-score map of two types, one being the map with GN and the other the map with AI. The abnormal side was judged by the maximum z score, which had to exceed 2, in the VOIs of the parahippocampal gyrus bilaterally.

Extent analysis

Extent analysis was also performed for each z-score map of both types, one being the map obtained with GN and the other that obtained with AI. Abnormalities were judged based on extent, that is, the ratio of the number of voxels which had z scores exceeding a z-score threshold to the total number of voxels in the VOI. The extent was computed by varying the z-score threshold by 0, 0.5, 1, 1.5 and 2. Subsequently, the

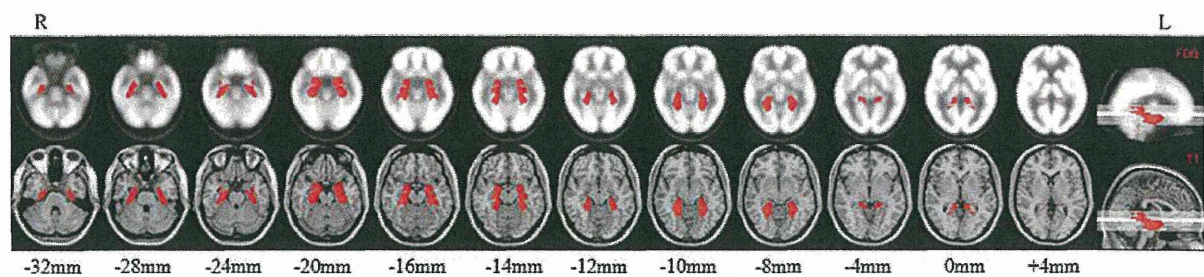


Fig. 2 A set of right and left volumes-of-interest (VOIs) in the parahippocampal gyrus was selected for determination of the side with the epileptogenic zone in a patient with mesial temporal lobe epilepsy. Transaxial and sagittal sections on the *upper row* indicate VOIs (*red regions*) on our in-house FDG template. The *lower images*

indicate VOIs (*red region*) on a spatially normalized T_1 -weighted magnetic resonance image. *Horizontal lines* on the sagittal sections correspond to transaxial slices displayed on the *left*. Numerical scales below the lower images show z coordinates on the Montreal Neurological Institute (MNI) space

side of the VOI exceeding the extent threshold was judged to be the abnormal side. In short, extent analysis was performed using two types of threshold: *z* score and extent. In this study, the abilities to accurately judge and determine optimum thresholds for *z* score and extent were evaluated as described in the following section.

Sensitivity, specificity and ROC analysis

The sensitivity and specificity of extent analysis were defined as follows. Sensitivity was the proportion of the number of patients in whom the side with the EZ was accurately judged as the abnormal side. Specificity was the proportion of patients in whom the non-abnormality was accurately judged on the side contralateral to the EZ. These sensitivity and specificity values were calculated by varying the extent threshold and used in the receiver operating characteristic (ROC) analysis. The ROC analysis was performed using the ROCKIT 1.1β2 program developed by Metz et al. [20] (<http://xray.bsd.uchicago.edu/krl>). The program calculates the area under the ROC curves (A_z), the statistical significance of the difference between the two A_z , accuracy, sensitivity and specificity. Accuracy and optimal threshold of extent were determined based on the value at the point at which sensitivity is the same as specificity on the ROC curve. Then, applying the PlotROC program (<http://xray.bsd.uchicago.edu/krl>), we drew ROC curves with the interpolated values statistically calculated. The extent analysis with AI at a *z*-score threshold of 0 was

excluded, because the extent of either right- or left-side VOI always exceeded 50% with this method.

Results

Peak analysis

The results of peak analysis are shown in Table 1. The rate of correct answers was better with the AI method than with the conventional GN method. For 12 patients in whom the side harboring the EZ was correctly identified using both the AI and the conventional method, the peak *z* scores were 6.2 ± 1.6 (mean \pm standard deviation) and 3.6 ± 1.0 , respectively, and the difference in peak *z* scores between the AI and conventional methods was significant by paired Student’s *t* test at $p < 0.001$ (two-tailed *p* value).

Extent analysis

The results of ROC analysis are shown in Table 2 and Fig. 3. Among all methods, the highest A_z of 0.971 was obtained at *z*-score thresholds of both 0.5 and 1 with the AI method. Applying the AI method at a *z*-score threshold of 0.5, the accuracy and the optimal extent threshold for judgment were 92 and 32.9%, respectively. With this extent threshold, the side harboring the EZ was correctly identified in 16 of 17 patients (94.1%). The extents at the ipsilateral and contralateral sides of the EZ were $70.3 \pm 22.3\%$ (mean \pm standard deviation) and $11.3 \pm 13.2\%$, respectively, such that the difference in extent between the sides ipsilateral and contralateral to the EZ was significant by paired Student’s *t* test at $p < 0.001$ (two-tailed *p* value). Applying the AI method at a *z*-score threshold of 1, the result of ROC analysis were also similar.

Among conventional GN methods, the highest A_z of 0.869 was obtained at a *z*-score threshold of 0.5, and the accuracy and the optimal extent threshold for judgment

Table 1 Results of peak analysis with *z*-score mapping

	Correct	Incorrect	Rate (%)
Global normalization	12	5	70.6
Asymmetry index	15	2	88.2

The number in the “Correct” or “Incorrect” column is the number of patients in which the side with the epileptogenic zone was or not correctly identified. “Rate” is the rate of correct identifications

Table 2 Receiver operating characteristic (ROC) curve results for the extent analysis

Asymmetry index						Global normalization				
Z	Extent-true (%)	Extent-false (%)	A_z	Ac (%)	Th (%)	Extent-true (%)	Extent-false (%)	A_z	Ac (%)	Th (%)
0	–	–	–	–	–	74.3 ± 22.6	33.2 ± 24.3	0.854	78	62.1
0.5	70.3 ± 22.3	11.3 ± 13.2	0.971	92	32.9	61.5 ± 23.7	19.9 ± 20.1	0.869	79	49.2
1	58.0 ± 24.7	5.7 ± 7.8	0.971	92	19.0	44.6 ± 23.4	10.6 ± 16.6	0.853	77	16.2
1.5	45.3 ± 25.4	2.5 ± 3.9	0.963	91	9.9	29.7 ± 20.7	5.7 ± 13.7	0.814	74	7.2
2	34.0 ± 23.4	1.0 ± 1.8	0.931	88	3.2	17.8 ± 15.5	3.1 ± 10.1	0.776	71	3.7

Values in “Extent-true” and “Extent-false” columns are presented as the mean \pm standard deviation. “Ac” and “Th” indicate the accuracy and threshold, respectively, for the extent analysis at the point at which sensitivity is the same as specificity on the ROC curve

Z *z*-score threshold, *Extent-true* extent on the side harboring the epileptogenic zone in a patient with MTLE, *Extent-false* extent on the contralateral side, A_z area under the ROC curve

were 79 and 49.2%, respectively. With this extent threshold, the side harboring the EZ was correctly identified in 14 of 17 patients (82.4%). No significant difference in A_z between the AI method at a z -score threshold of 0.5 and the conventional method at a z -score threshold of 0.5 was detected by the z -score test ($p = 0.1017$, two-tailed p value). Similarly, there was no significant difference in A_z between the AI method at a z -score threshold of 1 and the conventional method at a z -score threshold of 0.5, as demonstrated by the z -score test ($p = 0.1017$, two-tailed p value).

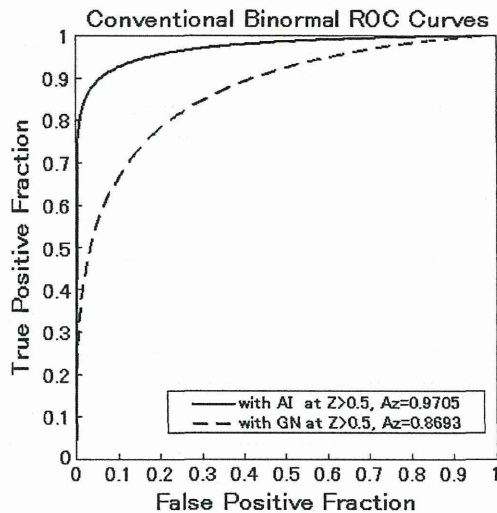


Fig. 3 Receiver operating characteristic (ROC) curves for the two methods employing the Asymmetry index (AI) and global normalization (GN) at the z -score threshold of 0.5

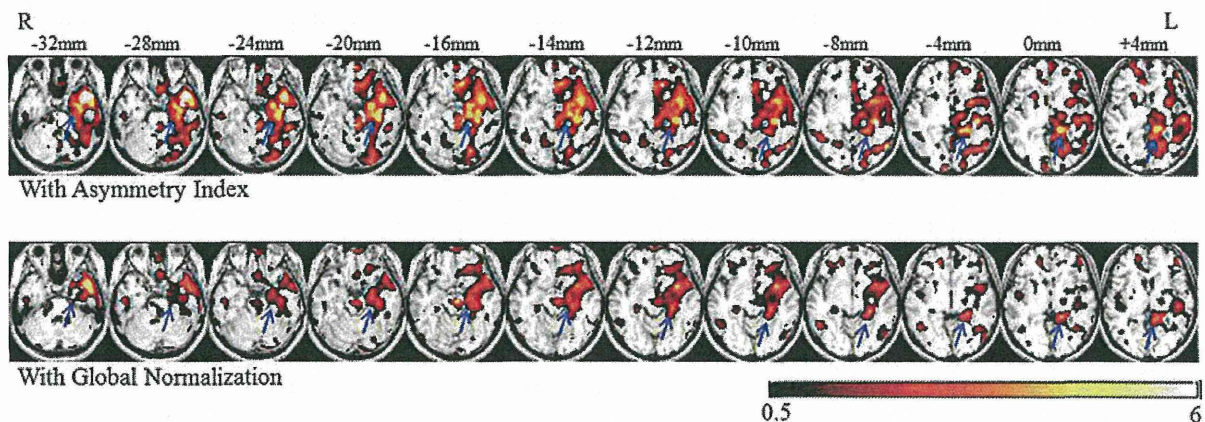


Fig. 4 Representative z -score maps obtained with the asymmetry index (AI *upper row*) and conventional global normalization (GN *lower row*) for comparison of FDG images from a patient with mesial temporal lobe epilepsy and controls. *Color-scaled* z -score maps are displayed as regions exceeding a z -score threshold of 0.5 on a spatially normalized T_1 -weighted magnetic resonance image. *Numerical scales above the upper images* show z coordinates on the

Representative z -score maps obtained by the AI and conventional GN methods are shown in Fig. 4.

Discussion

We applied AI, z -score mapping, and extent analysis techniques to preoperative FDG-PET in MTLTLE patients who were candidates for epilepsy surgery, and detected regional glucose hypometabolism. Moreover, we evaluated the detection utility of these methods to identify abnormalities in the unilateral hippocampal area later confirmed to harbor the EZ by surgical treatment and subsequent good seizure control. The AI method was more sensitive for detecting regional glucose hypometabolism and more accurate for identifying the EZ side than the conventional GN method. Automated identification of the side harboring the EZ showed improved accuracy with the combination of statistical z -score mapping employing AI and extent analysis based on VOIs of the parahippocampal gyrus.

Usefulness of SPM with AI

Similar to the results of previous studies on MTLTLE [10, 11], the AI technique was found to be more sensitive than the conventional GN technique for detecting regional glucose hypometabolism on unilateral PET images from MTLTLE patients as compared to those of a control group by automated analysis with a z -score peak (Table 1) and with extent analysis (Table 2; Fig. 3), although A_z values did not differ significantly between the AI and conventional methods.

Montreal Neurological Institute (MNI) space. This patient's epileptogenic zone is to the *left* of the parahippocampal gyrus. Peak z scores with AI and GN are 6.0 (*left side*) and 3.7 (*left side*), respectively, by peak analysis. Extents (*left side*) with AI and GN for this patient are 90.8 and 78.0%, respectively. Z -score mapping with the AI shows glucose hypometabolism in the parahippocampal gyrus (*arrow*) to be more severe and widespread than that mapped with GN

Laterality on FDG-PET images is a very important piece of information for radiologists making a clinical diagnosis. Conventional voxel-based analyses, such as SPM, the easy z-score imaging system (eZIS) [21] and three-dimensional stereotactic surface projections (3D-SSP) [22], detect differences in voxel values (employing voxel-value adjustment, as with GN, normalization of the cerebellum count, and normalization pertaining to other reference areas) between control and patient groups at the same coordinates. Thus, abnormalities cannot be detected, if the patient's voxel value is within the deviation of the control group's voxel values, even if abnormal laterality is seen in the patient's image. On the other hand, the method employing inter-hemispheric AI used in the present study can detect abnormal laterality in a patient if the AI of the patient's voxel value exceeds that of the control group's deviation in the AI of the corresponding voxel, even if the patient's voxel value is within the deviation of the control group's voxel values.

Usefulness of extent analysis

As noted in "Introduction", regional glucose hypometabolism is often observed as an extensive area associated with EZ rather than as a small area associated with an epileptic focus. Hence, we studied two indicators (peak and extent) for automated determination of the side harboring the EZ employing FDG-PET in patients with unilateral MTLE. In the present study, the highest accuracy was obtained employing the method combining AI and extent analysis (z -score threshold = 0.5, extent threshold = 32.9%, accuracy = 92% and the side harboring the EZ was correctly identified in 16 of 17 patients). Moreover, with both the AI and the GN method, the extent analysis yielded a higher rate of correct EZ-side identification than the peak analysis. It is conceivable that these improvement of accuracy depended on two benefits of the extent analysis. First of the benefits is robustness for statistical noise, because the number of target voxels in the extent analysis is more than that in the peak analysis. Second of the benefits is the approach for clinical background that an extensive area of glucose hypometabolism associated with EZ is observed. These results suggest that the extent analysis may provide important information for detecting the region of abnormal glucose hypometabolism. The usefulness of extent analysis for identifying this abnormal region as compared with the severity of the abnormality has been reported, although prior studies examined regional cerebral blood flow (rCBF) using SPECT in Alzheimer disease (AD). Mizumura et al. [23] stated that studying the extent of the region of abnormal rCBF causing functional disorders was more rational than assessing the severity of the rCBF abnormality reflecting local tissue degeneration. Matsuda et al.

[24] studied automated discrimination between very early AD patients and controls using three indicators (referred to as extent, severity and ratio) and noted in their report that the contention of Mizumura et al. may be supported by the fact that the discrimination power of the extent analysis was slightly higher than that of severity. Our present results, like those of both of the aforementioned reports, also showed the usefulness of extent analysis.

Technical limitations

Several technical limitations warrant discussion. First, in the present study, the normal control group was not age-, sex- and handedness-matched with each patient. Yanase and associates studied age-related FDG uptake using magnetic resonance imaging-based correction of the partial volume effect (PVE) [25]. Kawachi [26] and associates investigated sex and age differences and also inter-hemispheric laterality in cerebral glucose metabolism with a voxel-based analysis employing SPM in healthy right-handed volunteers. According to our literature search, there are no previous studies on inter-hemispheric laterality of glucose metabolism relevant to handedness. Whether there are age-, sex- and/or handedness-related inter-hemispheric AI changes in regional glucose metabolism remains uncertain, though several studies have raised these possibilities. Hence, for statistical analysis using AI of FDG-PET images, it is unknown whether or not an age, sex and handedness-matched control group is necessary.

The following (second, third and fourth) limitations were also mentioned by Didelot et al. [11]. Second, artifacts within a limited volume of several tens of voxels were centered over the inter-hemispheric midline, allowing AI to be used to generate a z -score map by applying a second spatial smoothing procedure to AI images. Such midline artifacts might hamper the interpretation of glucose hypometabolism in the mesial temporal lobe. However, these artifacts did not have a major impact in this study. The second spatial smoothing is related to FWHM; hence, further investigation of the influence of smoothing is necessary.

Third, the influence of symmetrization of the physiologically asymmetrical brain is unknown. Deformation of the brain, resulting from the normalization step for the symmetric template, differs between the left and right hemispheres. Brain deformation may influence the yield of AI analysis as a function of MTLE lateralization.

Fourth, the method employing AI cannot provide direct information as to whether an abnormal AI primarily reflects glucose hypermetabolism on one side or glucose hypometabolism on the other. In the case of bilateral MTLE, although not studied herein, the AI method might not provide adequate information about a bilateral absence